Earth Surf. Dynam. Discuss., https://doi.org/10.5194/esurf-2018-73
Manuscript under review for journal Earth Surf. Dynam.
Discussion started: 5 October 2018

Earth Surface Dynamics Discussions
Open Access
EGU

Displacement mechanisms of slow-moving landslides in response to changes in pore water pressure and dynamic stress

Jonathan M. Carey[1], Chris I. Massey[1], Barbara Lyndsell[1], David N. Petley[2]

[1] GNS Science, 1 Fairway Drive Avalon, PO Box 30368 Lower Hutt, New Zealand
[2] Department of Geography, University of Sheffield, Sheffield, S10 2TN, UK
Correspondence to: Jonathan M. Carey (j.carey@gns.cri.nz)

Abstract. Although slow-moving landslides represent a substantial hazard, their detailed mechanisms are still poorly understood. We have conducted a suite of innovative laboratory experiments using novel equipment to simulate a range of pore water pressure and dynamic stress scenarios on samples collected from a slow-moving landslide complex in New Zealand. We seek to understand how changes in pore water pressure and ground acceleration during earthquakes influence the movement patterns of slow-moving landslides. Our experiments show that during periods of elevated pore water pressure, displacement rates are influenced by two components: first, an absolute stress state component (normal effective stress state) and second, a transient stress state component (the rate of change of normal effective stress). During dynamic shear cycles, displacement rates are controlled by the extent to which the forces operating at the shear surface exceed the stress state at the yield acceleration point. The results indicate that during strong earthquake accelerations, strain will increase rapidly with relatively minor increases in the out of balance forces. Similar behaviour is seen for the generation of movement through increased pore water pressures. Our results show how the mechanisms of shear zone deformation control the movement patterns of many large, slow-moving translational landslides, and how they may be mobilised by strong earthquakes and significant rain events.

1 Introduction

Landslides are a significant natural hazard, responsible for up to 14,000 fatalities per annum globally (Petley, 2012; Froude and Petley, 2018). Although most fatalities occur during high velocity landslides, slow-moving landslides can cause high levels of loss. The movement of most non-seismic landslides is controlled by the effective stress state, but the relationship between pore water pressure and ground movement in slow-moving landslides is more complex than is often appreciated (Petley et al., 2017). In a few instances a simple (albeit non-linear) relationship between pore water pressure and movement rate has been observed (e.g. Corominas et al., 1999) allowing reasonable predictions of movement rate for any given pore water pressure. Conversely, in many cases much more complex relationships have been observed (e.g. Skempton, 1985; Corominas et al., 2005; Gonzalez et al., 2008, Carey et al., 2016), often involving hysteresis, for reasons that are poorly understood.

Earth Surf. Dynam. Discuss., https://doi.org/10.5194/esurf-2018-73
Manuscript under review for journal Earth Surf. Dynam.
Discussion started: 5 October 2018

To account for this complex behaviour it has been proposed that shear-strength parameters, represented as c' and phi' in the Mohr-Coulomb failure criterion, can be modified by inclusion of a viscous resistance component (Bertini et al., 1984; Leroueil et al., 1996; Corominas et al., 2005; van Asch, 2007; Picarelli, 2007; Gonzalez et al., 2008). However, whilst the use of viscosity functions may improve our understanding and ability to predict patterns of landslide movement by assuming that once motion is triggered, landslide displacement occurs as visco-plastic flow as opposed to frictional slip, such equations do not account for the pore water pressure and displacement hysteresis observed (e.g. Massey, 2010), requiring that the rate of movement reduces only when pore water pressures reduce. The observed hysteresis may be the result of a number of factors, including rate induced changes in shear strength of the materials (e.g. Lupini et al., 1981; Skempton, 1985; Angeli et al., 1996; Picarelli, 2007; Petley et al., 2017) or consolidation / strength regain during periods of rest (e.g. Angeli et al., 2004).

Landslide movement triggered by dynamic stress changes (i.e. during earthquakes) can also be complex. Many hillslopes fail during large earthquakes, and recent landslide inventories (e.g. Li et al., 2014; Valagussa et al., 2016; Massey et al., 2018) illustrate that factors such as shaking intensity and hillslope proximity to fault are key proxy for drivers of landslide movement. Despite this, many hillslopes adjacent to slopes that fail show limited downslope deformation despite high levels of local ground shaking and similar material and topographic characteristics (Collins and Jibson, 2015; Petley et al., 2006). Similarly, the post-seismic behaviour of these damaged hillslopes is poorly understood (e.g. Keefer, 1994; Hovius et al., 2011).

High quality measurement of earthquake-induced landslide movement is limited by the infrequency of high magnitude seismic events and the challenges of collecting real-time landslide monitoring data over appropriate coseismic and inter-seismic timescales. Therefore, coseismic landslide displacement is most commonly assessed using numerical modelling approaches (e.g. the Newmark Sliding Model - see Jibson, 2011 for example) which treat landslides as rigid blocks capable of movement when down-slope earthquake accelerations (based on acceleration time histories) exceed the basal frictional resistance (Newmark, 1965). These methods have provided reasonable estimates of earthquake induced landside activity (e.g. Dreyfus et al., 2013) and are widely applied in regional landslide hazard assessments (e.g. Wilson and Keefer, 1983), but they provide little insight into the processes occurring at the shear surface.

To date, v laboratory-based studies have attempted to consider how pore water pressure changes and seismic excitation influence slow-moving landslide displacement rates. To do so requires both high spatial and temporal resolution field monitoring data and laboratory testing that accurately replicates the complex stress conditions within slopes, a combination that is rarely available.

In New Zealand, slow-moving landslides are abundant in soft sedimentary rocks. The financial costs associated with their on-going movement are significant, particularly in agricultural areas where mitigation measures or slope management practices are rarely implemented (Mcoll and McCabe, 2016). These sedimentary rocks mostly comprise Neogene age, fine grained sandstones and mudstones, which cover approximately 17% of New Zealand's land surface (Fig 1a) (Massey et al., 2016). The New Zealand Landslide Database contains approximately 7,000 landslides within these sediments (Fig 1b) (Dellow et al., 2005; Rosser et al., 2017), the majority of which are relatively slow-moving, deep-seated, translational slides that reactivate frequently (Massey 2010).

Earth Surf. Dynam. Discuss., https://doi.org/10.5194/esurf-2018-73
Manuscript under review for journal Earth Surf. Dynam.
Discussion started: 5 October 2018

In this study we present a suite of laboratory experiments that simulate a range of pore water pressure and dynamic stress scenarios on samples of smectite-rich clay taken from the slide surface of the Utiku landslide, a very large, slow-moving slip. Such smectite-rich clays control many landslides in this area of New Zealand (Thomson, 1982; Massey, 2010). We compare the displacement patterns we observe in the laboratory to both high-resolution monitoring records collected from the landslide, along with numerical modelling of potential ground displacement during earthquakes, in order to get insights into the processes controlling the complex movement patterns observed at this location.

2 The Utiku Landslide Complex

The Utiku landslide complex, formed of early to mid-Pliocene Tarare sandstone and Taihape mudstone (Lee et al., 2012; Massey et al., 2013), is located in the central part of North Island, New Zealand (location 39.75°S, 175.83°E, Fig. 1a). According to the Hungr et al. (2014) scheme it is a reactivated, deep-seated translational landslide, with a volume of abo 2 x 10^6 m^3 (Massey et al., 2013). It has been studied since 1965, with high-resolution monitoring available since 2008. The landslide has generally moved slowly (varying between 16 mm/yr and 1.6 m/yr) (Stout, 1977), but it has repeatedly damaged the North Island Main Trunk railway (NIMT) and State Highway 1 (SH1), both of which cross the landslide (Fig. 1a and 1b).

2.2 Landslide displacements induced by pore water pressure increases

The Utiku landslide has been intensively studied using detailed field mapping, borehole analysis, evaluation of historical movements and the analysis of data from piezometers, inclinometers and rain gauges (Massey, 2010). The displacement time series (Fig. 1c) reveals complex behaviour dominated by periods of comparatively rapid movement, which can accumulate up to 120 mm of displacement per event at rates of up to 21 mm/day (Massey et al., 2013). These events coincide with seasonal peaks in pore-water pressure, with movement primarily associated with basal sliding (Fig. 1c). ile movement initiates with, and during periods of acceleration is controlled by, increases in pore water pressure, periods of deceleration are poorly correlated with pore water pressure value or any other monitored factor (Fig. 1d).

2.3 Earthquake induced landslide displacement

No episodes of monitored landslide movement to date can be attributed to earthquake shaking. Earthquake ground accelerations were recorded during the observation period, of which the largest (c. 1.0 m/s^2) had a >20-year return period (Massey et al. 2016).

Massey et al. (2016) simulated the response of the landslide to 14 earthquakes, whose accelerograms span the range and type of earthquakes that could affect the site, with Peak Ground Accelerations up to a 10,000 year return period (Stirling et al., 2012). The simulations adopted the decoupled method of Makdisi and Seed (1978), which is a modified version of the classic Newmark (1965) sliding block method that accounts for the dynamic response of the landslide mass as well as the permanent displacements accrued along the slide surface in response to the simulated earthquake. Massey et al. (2016) used

the relationship between the yield acceleration (K_Y) and the maximum average acceleration of the landslide mass (k_{max}), to determine the likely range of permanent displacements of the Utiku landslide in response to each of the 14 simulated earthquakes. K_Y effectively represents the increase in shear stress nee to reach the Mohr-Coulomb failure envelope of the slide surface-material. k_{max}, was used to represent the peak average acceleration experienced by a given landslide mass along a given slide surface, in response to the simulated earthquake. Thus, where $K_Y / k_{max} < 1.0$, the shear stresses along the simulated slide surface exceed the Mohr - Coulomb failure envelope of the slide surface material and permanent displacement can occur, with larger displacements occurring at lower ratios. $K_Y / k_{max} < 1.0$ r sents a factor of safety of 1.0. The simulated landslide mass will not move at K_Y / k_{max} ratios >1.0.

Annual frequencies of the peak ground accelerations (PGA) from each of the 14 simulated accelerograms were estimated from the hazard curve for the site assuming Site Class B (Rock) (NZS1170), and adopting the New Zealand National Seismic Hazard Model (Stirling et al., 2012). Using the method of Moon et al., (2005), Massey et al. (2016) estimated the mean annual permeant displacement of the landslide, concluding that the modelled mean landslide displacement rate in response to the simulated earthquakes is about 0.005–0.05 m/year, compared with historical and recent movement rates of the landslide (1972 to 2015), controlled by pore water pressure, that range from 0.04 to 0.07 m/year. The historical movement rates are similar to pre-historical rates (0.05–0.07 m/year) derived from radiocarbon dating and geomorphic indices. Thus, the results suggest that earthquake-induced displacements are not the driver of the long-term movement rate of the Utiku landslide.

3 Material characteristics and laboratory methods

3.1 Material sampling and physical properties

To obtain representative North Island Neogene mudstone samples a 3 m deep trench was excavated into the active shear zone in lower section of the Utiku landslide complex (Fig 1a). To minimise sample disturbance and maintain field moisture conditions block samples were hand-dug from trench walls before being packaged and transported to the GNS labor ies for testing.

Physical properties tests demonstrated that this material has a natural moisture content of 27.5% with a liquid limit of 80% and plastic limit of 37% (Table 1). The Atterberg limits indicate the mudstone is close to the boundary between very high plasticity silt and very high plasticity clay (defined in accordance with BS5930 (BSI 1990).

3.2 Shear box experiments

A suite of shear experiments was conducted in a Dynamic Back-Pressured Shear Box (DBPSB). The DBPSB is highly modified direct shear device, constructed by GDS Instruments Ltd and described in detail by Brain et al. (2015) and Carey et al. (2016; 2017). The apparatus can function as both a conventional direct shear and back-pressured shear machine and provides both static and dynamic control of horizontal (shear) and axial (normal) force and displacement; total stress; and effective stress. In addition, sample pore water pressure can be monitored throughout each experiment.

Earth Surf. Dynam. Discuss., https://doi.org/10.5194/esurf-2018-73
Manuscript under review for journal Earth Surf. Dynam.
Discussion started: 5 October 2018

Samples were fully saturated to simulate the shear zone conditions within the landslide complex during periods of movement using the methodology previously described by Carey et al. (2016). Consolidation was undertaken at effective stresses of 150 kPa and 400 kPa by maintaining the total normal stress after saturation and reducing the back pressure. The normal load was applied through a feedback controlled actuator that permitted the control of stress and sample displacement.

Following consolidation, three samples (UTA, UTB and UTC) were subject to an initial drained direct shear test (Table 1) to determine the Mohr Coulomb strength envelope of the soil, and to generate a pre-existing shear surface for further testing. A slow displacement rate (0.001 mm/min) was used to prevent the development of excess pore-water pressures, and a full shear reversal was completed on each sample to ensure residual strength was achieved.

A series of tests were then undertaken under representative field stress paths often termed pore pressure reinflation (PPR) tests (Petley et al., 2005). To replicate deep shear surface depths an initial confining pressure of 400 kPa was applied to sample UTB and 150 kPa applied to samples UTC and D. These initial confining pressures were held constant whilst a shear stress of 75 % of residual shear strength at each confining pressure (95 kPa and 52 kPa) was applied, ramped at a rate of 1 kPa / hr to avoid the generation of excess pore water pressures (Fig 2a).

To simulate the development of a first-time failure, sample UTD was subjected to a linear PPR test until failure occurred. The back pressure (applied pore water pressure) was raised at a rate of 5 kPa / hr, while the shear and total normal stresses were held constant (Fig 2a and b) and sample horizontal (shear) displacement and pore water pressure development were monitored. After failure, the excess pore water pressure was allowed to dissipate and a conventional drained shear was undertaken. This experiment was then repeated to investigate the behaviour of a fully formed shear surface (Table 2).

To explore the displacement response of the landslide shear surface to increasing and decreasing pore water pressures, samples UTB and UTC were subjected to different patterns pore water pressure change at constant total normal and shear stresses (Figs 2a and c). To measure the deformation response of the shear zone when pore pressures were increasing and decreasing linearly both samples were initially subjected to a linear increase in back pressures (applied pore water pressure) at a rate of 5 kPa / hr to a pre-determined displacement limit of 6 mm, whereupon the back pressure was reduced at the same rate to the initial back pressure (100 kPa). To simulate more complex changes in the shear surface pore water pressure a stepped pattern of back-pressure increases and decrease was applied to sample UTC over a similar time period. Between the linear PPR and stepped PPR tests for sample UTC, the conventional shear strength was measured during the shear reversal in order to determine whether any shear stress reduction occurred during the test stage (Table 1).

To simulate different amplitudes of earthquake shaking we undertook a suite of dynamic shear experiments using samples UTC, E and F (Table 3). Each sample was tested with an initial normal effective stress of 150 kPa, and an initial shear stress of 20 kPa, representing a stable slope condition. Following the initial shear stage, each sample was subjected to a series of dynamic, shear stress-controlled experiments at constant normal stress and back pressure (Fig. 2d, e and f). During each dynamic experiment a different maximum shear stress was applied to the sample and the horizontal (shear) displacement and pore water pressure response of the sample were measured.

A single dynamic shear experiment was undertaken on sample UTC (Table 3), at a frequency of 1 Hz for a duration of 60 s (i.e. 60 cycles in total), to assess the behaviour of a landslide shear surface previously subjected to rainfall-induced failure (Table 2). To assess the behaviour of a landslide shear surface during a large earthquake event and subsequent aftershocks (Table 3), sample UTE was subjected to a large initial dynamic shear experiment (DYN1) at 1 Hz for a duration of 60 s (60 cycles per test). The shear box was then reversed and the initial stress conditions were re-applied to the sample before four further dynamic shear stress experiments were carried out at the same frequency (Table 3). A further 14 dynamic shear experiments were undertaken on sample UTF at a frequency of 2 Hz (120 cycles per test) to characterise progressive landslide behaviour during multiple dynamic events (Table 3).

To compare the results from the laboratory experiments with the simulated landslide displacements from Massey et al. (2016), we converted the permanent displacements in the laboratory measurements and numerical simulations into strain, and the static and dynamic shear stress acting on the mass of the laboratory sample and simulated slide surface into acceleration. For each experiment we: (1) calculated the permanent displacement per cycle during each dynamic shear experiment; (2) calculated the mass of the sample under the applied static normal stress, which remained constant for all tests; (3) derived the yield acceleration of the sample from the initial stress state, of each experiment, from the force (shear stress) applied to the sample to reach the conventional failure envelope; and (4) derived the maximum amplitude of acceleration from the maximum force (shear stress) applied during each experiment, which we assume to be equivalent to k_{max}.

4 Results and discussion

4.1 Drained shear behaviour

The drained shear experiments demonstrate a clear reduction in shear stress during each stage, which indicates progressive softening of the clay to residual state (Fig. 3a). The final shear stress at the end of each initial shear stage was used to calculate a residual Mohr-Coulomb strength envelope (ϕ=11.3°, c=30 kPa, Fig. 3b). The residual strength parameters calculated from ring shear experiments on shear zone samples in the landslide (Kilsby, 2007) indicate ϕ=8.5° and c=4-10 kPa. Given that ring shear experiments typically produce parameters slightly lower than those determined from shear box experiments (Skempton, 1985), we infer our results to be broadly consistent with these previous measurements, although the difference in cohesion is notable. However, the ring shear experiments used samples that had been completely remoulded, whereas the shearbox samples were intact. This probably explains the difference, and we consider that the shearbox results are more likely to represent material behaviour at the landslide shear surface.

4.2 Deformation response to changes in pore water pressure

Experiments UTD PP1 and UTD PP2 demonstrated different behaviour during first-time failure (UTD PP1) and post-failure (UTD PP2) remobilisation of the shear surface (Fig 4). During first time failure the sample showed brittle failure, in common with previous studies of mudstones (Carey and Petley 2014). Measurable displacement was characterised by initially low

displacement rates from initiation at a critical normal effective stress, thereafter increasing exponentially with increasing pore water pressure (reducing mean effective stress) (Fig. 4b). This behaviour produces an asymptotic trend in 1/v – t space (Fig. 4c) and is indicative of plastic deformation during the secondary creep phase (Petley et al., 2005). As pore water pressures continued to increase a hyperbolic increase in displacement rate developed (Fig 4b), characterised by a linear trend in 1/v - t space to final failure (Fig 4c), indicative of brittle failure processes.

Sample UTD PP2 explored failure on an existing shear surface (created in experiment UTD PP1). Although shear displacement initiated at a similar normal effective stress (Fig. 4d), the displacement rate remained comparatively low as pore water pressure increased (Fig. 4e). As the shear strain developed the rate of displacement was moderated by a reduction in the rate of pore water pressure increase, probably indicating dilation (Fig. 4e). As a consequence, the displacement rate increas in a complex, non-linear manner with increasing pore water pressure, as indicated by an asymptotic trend in 1/v - t space (Fig. 4f.) Similar behaviour has been observed in non-brittle landslide materials (Petley et al., 2017; Carey et al., 2015) and in remoulded materials (Ng and Petley, 2009; Carey and Petley, 2014). Thus, behaviour is conventional as a brittle first time failure and followed by ductile reactivation.

In response to linear increases in pore water pressure, displacement for the samples with pre-existing shear surfaces (experiments UTB PP1 and UTC PP1) initiated at a critical normal effective stress / pore-water pressure threshold (Figs 5a and b). In both samples further increases in back pressure generated a rapid increase in displacement rate (Figs 5c and d). During this phase of movement, the rate of pore water pressure increase lagged the applied back pressure, indicating that the porosity of the shear surface zone increased as the sample dilated. In both experiments we observed similar peak displacement rates (0.007 mm min^{-1}), which were reached while pore water pressures were still increasing. Thereafter, the two samples demonstrated different displacement patterns. Sample UTB PP1showed a decreasing trend in displacement rate before the peak pore-water pressure was reached (Fig. 5e), whilst UTC PP1 showed a fluctuating, but near constant, displacement rate before peak pore water pressure was reached (Fig. 5 f). In both experiments a reduction in the rate of increase of pore water pressure was observed as the shear surface mobilised, indicating that the shear zone dilated as the sample sheared, resulting in local dissipation of pore water pressures within the thin shear band.

A complex relationship between shear surface deformation and pore-water pressure was explored with a stepped PPR experiment (UTC PP2) (Figs 6a and b). The rapid increase in back pressure during stage 1 (Fig. 6b) resulted in a lag in the pore water pressure response, which we infer to be associated with low sample permeability. The change in pore water pressure induced an initial rapid increase in displacement rate, followed by a reduction in rate as pore water pressures equilibrated (Fig. 6b). Thus, the displacement rate shows a transient component associated with a change in the pore water pressure. As the stress state equilibrates the transient displacement rate component declines.

A further stepped increase in pore water pressure (stage 3) induced an associated transient increase in displacement rate (Figs 6b and c). The displacement rate rapidly declined however, even whilst applied pore water pressure (back pressure) was held stable (Figs 6b and c, stage 4) and measured pore water pressure continued to rise.

Earth Surf. Dynam. Discuss., https://doi.org/10.5194/esurf-2018-73
Manuscript under review for journal Earth Surf. Dynam.
Discussion started: 5 October 2018

In stage 5 pore water pressure was ramped down; at this point the rate of displacement rapidly declined to zero (Figs 6b and c). In Stage 6 the pore water pressure was held constant at a value greater than that at the initiation of displacement in this experiment. No displacement was recorded in this stress state. This behaviour of movement initiating at a lower pore water pressure than was the case when movement ceased was consistent in both the linear PPR and stepped PPR experiments. The resultant hysteretic relationship between pore water pressure and displacement rate (Figs 5e, 5f and 6c) was also observed within the landslide complex during periods of accelerated displacement (Massey et al., 2013).

4.2.1 Implications for landslide movement

Our experiments demonstrate a complex relationship between pore water pressure and displacement rate. The controlling factor appears to be a function of both the instantaneous pore water pressure value (i.e. the mean effective stress at that time) at the landslide shear surface and the rate of change of pore water pressure (i.e. the rate of change of normal effective stress). Given that, by definition, a change in stress must result in strain, two components of shear strain can be defined: first, the stress state component (σ'_n) and second, a transient stress state component defined by the change in normal effective stress state ($\Delta \sigma'_n$). This relationship can be expressed using Eq. (1):

$$v = \sigma'_n + \Delta \sigma'_n \quad (1)$$

where v is the displacement rate, σ'_n is the normal effective stress applied to the sample by increasing pore water pressure a $\Delta \sigma'_n$ represents the rate of change in normal effective generated by increasing pore water pressure.

We present a conceptual model (Fig. 7) to illustrate how this relationship controls landslide displacement during periods of elevated pore water pressure. The model shows that as pore water pressure increases the landslide remains stable until the mean effective stress is reduced to a critical condition at which displacement can occur (Fig. 7 stage A1). Once this movement is initiated the landslide displacement rate is a function of both the mean effective stress (background displacement rate component), and the rate of change of pore water pressure (transient displacement rate component). During periods when pore water pressures are constant, the rate of displacement is defined simply by the effective stress state. However, in periods of transient pore water pressures the displacement rate will be a combination of this stress state plus that generated by the changing stress state (Fig. 7 stage A2). A further increase in pore water pressure (reduction in mean effective stress) generates both a new stress state and a transient motion resulting in higher landslide displacement rates (Stage B1, C1). When the effective stress state stabilises (Fig. 7 Stage B2, C2,) the displacement rate reduces to its non-transient value. As pore water pressures reduce (mean effective stress increases) the negative change in pore water pressure produces a negative transient strain rate and consequently landslide displacement rates rapidly decline (Fig. 8 Stage D3).

The style of deformation described is consistent with ground movement responses measured within the Utiku landslide during periods of elevated pore water pressure (Massey et al., 2013). Movement rates clearly increased when the

pore water pressure increased. However, movement rates rapidly declined when pore water pressures plateaued, and reduced to zero as soon as pore water pressures started to reduce. Thus, the behaviour is consistent in the field and the laboratory. Experiments on a silt from Lantau Island in Hong Kong showed similar behaviour (Ng and Petley, 2009; Petley et al., 2017). Furthermore, we speculate that this behaviour may also be consistent with the movement patterns observed in other slow-moving landslides, such as 'stick-slip' behaviour (e.g. Allison and Brunsden, 1990).

4.3 Deformation during dynamic shear experiments

To characterise the displacement mechanisms in response to seismic excitation we undertook a series of dynamic shear experiments at a constant normal effective stress of 150 kPa (chosen to be representative of the normal stress state in the landslide) on samples UTC, UTE and UTF (Fig 8).

To evaluate how first-time failure may develop during seismic excitation, intact sample UTE was subject to a dynamic, large amplitude, shear stress designed to significantly exceed the conventional failure envelope (Fig. 8a). A maximum shear stress of 120 kPa was reached during the first dynamic cycle (within 0.5 s), resulting in displacement response of 8 mm over the same time period, indicating that the shear surface formed rapidly (Fig. 8b). This rapid displacement coincided with an initial increase in normal effective stress (Fig. 8c), which suggests that the sample dilated, before subsequent cycles generated excess pore water pressure (Fig. 8b), reducing the normal effective stress significantly (Fig. 8c). Permanent displacement of the sample occurred at an approximately constant net rate per cycle until the experiment terminated within four cycles (3.5 s^{-1}), the machine having reached its pre-set displacement limit (14 mm).

We observed that during experiments in which the applied maximum shear stress exceeded the conventional failure envelope, such as UTE DYN5 (Figs. 8d, e and f), and UTF DYN12 (Figs. 8g, h, i) movement initiated and resulted in permanent displacement at a near-constant (actually slightly declining) displacement rate per cycle (Figs 8e and h). In each case we observed that displacement rates increased at higher shear stresses and generated higher excess pore water pressure (lower mean effective stresses) (Fig 8b, e, h). Experiments in which shear stresses did not exceed the monotonic failure envelope, such as UTE DYN2 (Fig. 8f) and UTF DYN2 (Fig 8i) displayed either no displacement or extremely low displacement rates, and there were negligible changes in pore water pressure (Figs 8e and h respectively).

Using the method proposed by Brain et al. (2015), we use the average normal effective stress and the maximum shear stress (Fig. 9a) to plot displacement rates against the distance normal to the failure envelope during each experiment (Fig. 9b). This shows that dynamic stress changes that do not reach the conventional failure envelope generate negligible amounts of displacement. On the other hand, dynamic stress states that reach or exceed the failure envelope generate displacement rates that increase exponentially with distance normal to the conventional failure envelope (Fig. 9b). This relationship remains statistically valid for all samples tested, regardless of the initial stress state imposed, their stress history and frequency of seismic excitation applied. This demonstrates that the shear zone behaviour is controlled by a conventional Mohr-Coulomb relationship, indicating that the material strength characteristics remain constant and are not subject to strain hardening, weakening or rate effects. In Fig. 9c we have added the peak displacement rates for the PPR experiments, using the same

methodology. These experiments show that these experiments generate significantly lower displacement rates than the trend for the dynamic tests. The later involve large, rapid changes in stress state (in this case shear stress), whereas the PPR experiments involve a much smaller rate of change in stress state. Thus, we would expect to have a much higher transient component to the displacement rate in the dynamic tests.

4.3.1 Implications for landslide movement

Our results suggest that the materials that form the Utiku landslide are not susceptible to liquefaction. Instead dynamic shear stresses that exceed the conventional failure envelope of the sample generate out of balance forces that trigger permanent displacement. The magnitude of displacement that occurs is a function of the magnitude and duration of the force imbalance. These results are consistent with previous studies, which consider more complex wave forms (Brain et al., 2015). We infer from our results that the frictional properties of the materials we tested do not increase (strain harden) or decrease (strain weaken) but remain constant during seismic excitation, in the dynamic stress ranges examined. We anticipate, therefore that the relationship between displacement rate and normal distance from the failure envelope would also be observed for complex seismic wave forms, but this requires further investigation.

Figure 10 shows the calculated strain for different K_Y / k_{max} ratios derived from the dynamic laboratory experiments reported here and from the numerical simulations from Massey et al. (2016). Both datasets can be described by power law functions indicating that strain increases rapidly with decreasing K_Y / k_{max} ratios, showing that the tested material and the simulated landslide strains are both controlled by the amplitude of earthquake acceleration above the yield acceleration. The curves do not coincide perfectly as the lab and field tests started from a different stress state.

Although very large accelerations cannot be simulated in the laboratory equipment, the power laws fitted to both data sets (Fig. 10) indicate that during strong earthquake accelerations strain will increase rapidly with relatively minor reductions in the K_Y / k_{max} ratio. From this we infer that the tested material and simulated landslide would undergo large strains (displacements) when accelerated by strong earthquakes.

These results show that dynamic changes in shear stress, which exceed the monotonic failure envelope of the shear surface material, result in permanent landslide displacement and movement rates several orders of magnitude greater than would be anticipated by similar magnitudes of normal effective stress reduction during periods of elevated pore water pressure. However, Massey et al. (2016), show that the frequency of such large earthquake accelerations in the Utiku area is low, such that over the lifetime of the landslide most of the movements are associated with changes in pore water pressure. In an area with a higher occurrence of large magnitude earthquakes, landslide behaviour would be more affected by co-seismic displacements.

4.4 Understanding the movement of the Utiku Landslide Complex

Our data suggest that the clay seams controlling the movement of the Utiku landslide behave in a conventional manner, with no rate and state dependent friction characteristics. The landslide itself moves on a quasi-planar shear surface, with

comparatively low variation in thickness, rendering its behaviour comparatively simple. This makes it an ideal mass for which to explore response to pore water pressure and earthquake shaking.

In the experiments in which we explore response to pore water pressure we find that the landslide starts to accumulate strain before the conventional residual Mohr Coulomb failure envelope is reached. We interpret this behaviour to be creep, in common with other studies (Petley et al., 7). In this phase, the rate of movement is controlled by pore water pressure, and there is a transient behaviour in response to changes in effective stress. This transient behaviour leads to a marked hysteresis in response to fluctuating pore water pressure, observable because the background strain rates are low.

Once the stress path reaches the failure envelope, the rate of movement is controlled by the out of balance forces. These experiments do not show classical critical state behaviour; instead the stress path can exceed the failure envelope. In common with the results of Brain et al. (2015), we find that the rate of strain is determined by the normal distance from the shear surface, which is a proxy for the magnitude of the out of balance force.

The same style of behaviour is seen in the dynamic tests. In this case, a strong correlation is seen between the maximum distance from the failure envelope in each cycle and the accumulated strain. Thus, the strain behaviour is controlled, and can be described, by understanding the stress path of the shear surface. The key modification is creep behaviour below the failure envelope, and the role of transient creep during periods of pore water pressure change.

Our alternative approach to examining the behaviour of the Utiku landslide invoked the k_Y/k_{max} analysis of Massey et al. (2016). In essence the yield acceleration can be considered to be the point at which the factor of safety reaches unity, whilst k_{max} is the maximum acceleration – i.e. the maximum shear stress. Thus, the two approaches are describing the same stress state. Thus, the k_Y/k_{max} analysis also suggests that the static and dynamic behaviour of the Utiku landslide can be described using a conventional Mohr Coulomb approach so long as the stress path is known.

In the case of Utiku, seismic accelerations can take the landslide into a state in which large strains can accumulate. However, in this case the frequency of such strong earthquakes occurring is low, such that little of the large accumulated displacement to date is likely to have originated from this mechanism. Displacements associated with elevated pore water pressures are much smaller, but occur frequently. The laboratory tests corroborate the results of Massey et al. (2016), that the cumulative effect of pore water pressure-induced displacements over the life of the landslide is large, such that the total displacement to date is likely to have been dominated by the effects of elevated pore water pressures.

5 Conclusion

In our study we have used a dynamic back pressured shear box to simulate representative stress conditions in a slow-moving landslide in Neogene mudstones during phases of pore water pressure fluctuation and seismic excitation. The results provide new insight into their movement mechanisms: -

1. While catastrophic landslides can o[ccur] though brittle shear surface development during large earthquakes and rainfall events, reactivations of existing landslide shear surface are unlikely to generate catastrophic failure unless topographically permitted.
2. During periods of elevated pore water pressure, displacement rates are influenced by two components: First, an absolute stress state component (normal effective stress) and second, a transient stress state component (the rate of change of normal effective stress). The behaviour observed in the laboratory is consistent with the ground monitoring records ar[e] explains the differing relationships between displacement rate and pore water pressure during periods of acceleration and deceleration in some slow-moving landslides.
3. During dynamic shear we show that displacement rates are controlled by the extent to which the forces operating at the shear surface are out of balance. Once these forces exceed the yield acceleration, displacement rates increase rapidly with distance n[orm]al to the failure envelope in plots of shear stress against normal effective stress.
4. The combined laboratory and numerical simulation indicate that during strong earthquake accelerations, strain will increase rapidly with relatively minor increases in the out of balance forces (reducing the K_Y/k_{max} ratio). Therefore, we anticipate that large landslide displacements could occur when accelerated by strong earthquakes, but such accelerations in the study area do not occur frequently. Thus, in this area over long (i.e. multiple seismic cycle) timescales landslide displacement is predominantly controlled by pore water pressures

By combining the specialised laboratory testing with field monitoring, well-constrained ground models and numerical simulations, we have shown how the mechanisms of deformation occurring along a landslide shear surface control the movement patterns of many large, slow moving translational landslides. The development of such approaches provides a framework, which can be used in complex hazard assessment of landslides that could be mobilised by both strong earthquakes and significant rain events.

Acknowledgements

This research has been undertaken with Financial support provided by EQC Bi-annual Grant 16/721, the GNS Science Investment Funding and by the NERC/ESRC Increasing Resilience to Natural Hazards programme, grant NE/J01995X/1, and NERC/Newton Fund grant NE/N000315. We thank GNS Science staff Stuart Read and Zane Bruce for laboratory support and Dr Mauri McSaveney for his helpful discussions and suggestions throughout the study.

References

Allison, R., and Brunsden, D.: Some mudslide movement patterns. Earth Surface Processes and Landforms., 15, 297-311, 1990.

Angeli, M.G., Gasparetto, P., and Bromhead, E.: Strength-regain Mechanisms in Intermittently Moving Landslides. Proceedings of the 9th International Symposium on Landslides. Rio de Janeiro., 1, 689-696, 2004.

Angeli, M.G., Gasparetto, P., Menotti, R.M., Pasuto, H., and Silvano, S.: A visco-plastic model for slope analysis applied to a mudslide in Cortina d'Ampezzo, Italy. The Quarterly Journal of Engineering Geology and Hydrology., 29, 233-240, 1996.

Bertini, T., Cugusi, F., D'Elia, B., and Rossi-Doria, M.: Climatic Conditions and Slow Movements of Colluvial Covers in Central Italy, Proceedings of the IV International Symposium on landslides, Toronto., 1, 367–376, 1984.

Brain, M.J., Rosser, N.J., Sutton, J., Snelling, K., Tunstall, N. and Petley, D.N.: The effects of normal and shear stress wave phasing on coseismic landslide displacement. Journal of Geophysical Research: Earth Surface., 1009-1022, 2015.

British Standards Institute (BSI).: British standard methods of test for soils for civil engineering purposes. Part 1: General requirements and sample preparation. BS 1377: Part 1. Board. US National Research Council, Washington, DC., 36–75 Special Report 247, 1990.

Carey, J.M., and Petley D.N.: Progressive shear-surface development in cohesive materials; implications for landslide behaviour, Engineering Geology., 177, 54-65, 2014.

Carey, J.M., Moore, R., and Petley, D.N.: Patterns of movement in the Ventnor landslide complex, Isle of Wight, southern England. Landslides., 12(6), 1107-1118, 2015.

Carey, J.M., McSaveney, M.J., Lyndsell, B.M., and Petley, D. N.: Laboratory simulation of a slow landslide mechanism. p. 557–564. In, Aversa, S.; Cascini, L.; Picarelli, L.; Scavia, C. (eds) Landslides and engineered slopes: experience, theory and practice: proceedings of the 12th International Symposium on Landslides, Naples., 2, 557-564, 2016.

Carey, J.M., McSaveney, M.J., and Petley, D.N.: Dynamic liquefaction of shear zones in intact loess during simulated earthquake loading, Landslides., 14(3), 789-804, 2017.

Collins, B. D., and Jibson, R.: Assessment of existing and potential landslide hazards resulting from the April 25, 2015 Gorkha, Nepal earthquake sequence, Report Rep., 2015-1142, 2015.

Corominas, J., Moya, J., Ledesma, A., Lloret, A., and Gili, J.A.: Monitoring of the Vallcebre landslide, Eastern Pyrenees, Spain. Proceedings of the International symposium on Slope Stability Engineering. IS-Shikoku' 99. Matsuyama. Japan., 1239–1244, 1999.

Corominas, J., Moya, J., Ledesma, A., Lloret, A., and Gill, J.A.: Prediction of Ground Displacements and Velocities from Groundwater Level Changes at the Vallebre Landslide (Eastern Pyrenees, Spain). Landslides., 2, 83-96, 2005.

Dellow, G.D., McSaveney, M.J., Stirling, M.W., and Berryman, K.R.: A Probabilistic Landslide Hazard Model for New Zealand, p. 24. In: Pettinga, J.R., Wandres, A.M. (eds.), Geological Society of New Zealand 50th Annual Conference, 28 November to 1 December 2005, Kaikoura: Programme & Abstracts, 119A. Geological Society of New Zealand Miscellaneous Publication., 2005.

Dreyfus, D., Rathje, E.M., and Jibson, R.W.: The influence of different simplified sliding-block models and input parameters on regional predictions of seismic landslides triggered by the Northridge earthquake, Engineering Geology., 163, 41–54, 2013.

Froude, M., and Petley, D.N.: Global fatal landslide occurrence 2004 to 2016, Natural Hazards and Earth System Science., 18, 2161-2181, 2018.

Gonzalez, D.A., Ledesma, A., and Corominas, J.: The viscous component in slow-moving landslides: a practical case. In: Chen et al. (ed,), Landslides and Engineering Slopes., 237-242, 2008.

Hovius, N., P. Meunier, C.-W. Lin, H. Chen, Y.-G. Chen, S. Dadson, M.-J. Horng, and M. Lines.: Prolonged seismically induced erosion and the mass balance of a large earthquake, Earth Planet. Sci. Lett., 304(3–4), 347–355, 2011.

Hungr, O., Leroueil, S., and Picarelli, L.: The Varnes classification of landslide types, an update, Landslides., 11, 167-194, 2014.

Jibson, R. W.: Methods for assessing the stability of slopes during earthquakes—A retrospective, Engineering Geology., 122(1–2), 43–50, 2011.

Keefer, D. K.: The importance of earthquake-induced landslides to long-term slope eroion and slope-failure hazards in seismically active regions, Geomorphology., 10(1), 265–284, 1994.

Kilsby, C.: An engineering geological appraisal of the Utiku Landslide, North Island, New Zealand. University of Portsmouth, MSc Thesis., 2007.

Lee, E.M., Bland, K.J., Townsend, D.B., and Kamp, P.J.J.: Geology of the Hawkes Bay area. Institute of Geological and Nuclear Sciences 1:25,000 geological map 8. Lower Hutt. Institute of Geological and Nuclear Sciences Limited., 2012.

Leroueil, S., Locat, J., Vaunat, J., Picarelli, L., and Faure. R.: Geotechnical characterisation of slope movements. In. Proceedings of the Seventh International Symposium on Landslides, (Ed. Sennest) Trondheim, Norway, Balkema, Rotterdam., 1, 53-74, 1996.

Li, G., West, A.J., Densmore, A.L., Jin, Z., Parker, R.N., and Hilton, R.G.: Seismic mountain building: Landslides associated with the 2008 Wenchuan earthquake in the context of a generalized model for earthquake volume balance, Geochem. Geophys. Geosyst., 15, 833–844, 2014.

Lupini J.F., Skinner A.E., and Vaughan P.R.: The drained residual strength of cohesive soils: Geotechnique., 31(2), 181-213, 1981.

Makdisi, F.I., and Seed, H.B.: Simplified procedure for evaluating embankment response. Journal of Geotechnical Engineering Division. American Society of Civil Engineers., 105(GT12), 1427–1434, 1978.

Massey, C. I.: The dynamics of reactivated landslides: Utiku and Taihape, North Island, New Zealand. PhD thesis, Durham University., 2010.

Massey CI, Petley DN, McSaveney MJ (2013) Patterns of movement in reactivated landslides. Engineering Geology, 159: 1-19.

Massey, C.I., Abbott, E.R., McSaveney, M.J., Petley, D.N., and Richards, L.: Earthquake-induced displacement is insignificant in the reactivated Utiku landslide, New Zealand. In, Aversa, S.; Cascini, L.; Picarelli, L.; Scavia, C. (eds) Landslides and engineered slopes: experience, theory and practice: proceedings of the 12th International Symposium on Landslides. Boca Raton, Fla., 31–52, 2016.

Massey, C.I., Townsend, D.B., Rathje, E., Allstadt, K.E., Lukovic, B., Kaneko, Y., Bradley, B., Wartman, J., Jibson, R.W., Petley, D.N., Horspool, N.A., Hamling, I.J., Carey, J.M., Cox, S.C., Davidson, J., Dellow, G.D., Godt, G.W., Holden, C., Jones, K.E., Kaiser, A.E., Little, M., Lyndsell, B.M., McColl, S., Morgenstern, R.M., Rengers, F.K., Rhoades, D.A., Rosser, B.J., Strong, D.T., Singeisen, C., and Villeneuve, M.: Landslides triggered by the 14 November 2016 Mw 7.8 Kaikoura earthquake, New Zealand. Bulletin of the Seismological Society of America., doi: 10.1785/0120170305, 2018.

Mcoll, S.T., and McCabe, M.: The causes and Agricultural impacts of large translational landslides: Case studies from North Island, New Zealand. In, Aversa, S.; Cascini, L.; Picarelli, L.; Scavia, C. (eds) Landslides and engineered slopes: experience, theory and practice: proceedings of the 12th International Symposium on Landslides. Boca Raton, Fla., 1401-1408, 2016

Moon, A.T., Wilson, R.A., and Flentje, P.: Developing and using landslide size frequency models. http://ro.uow.edu.au/engpapers/384, 2005.

Newmark, N.: Effects of earthquakes on dams and embankments, Geotechnique., 15, 139–160, 1965.

Ng, K-Y., and Petley, D.N.: A process approach towards landslide risk management in Hong Kong, Quarterly Journal of Engineering Geology and Hydrogeology., 42 (4), 487-498, 2009.

Petley, D.N., Higuchi, T., Bulmer, M.H., Carey, J.: The development of progressive landslide failure in cohesive materials, Geology., 30, 719-722, 2005.

Petley, D. N., Dunning, S.A., Rosser, N.J., Kausar, A.B.: Incipient landslides in the Jhelum Valley, Pakistan following the 8th October 2005 earthquake. In, Marui, H. (ed) In Disaster Mitigation of Debris Flows, Slope Failures and Landslides, Universal Academy Press, Tokyo., 47-56, 2006.

Petley, D.N.: Global patterns of loss of life from landslides, Geology., 40(10), 927-930, 2012.

Petley, D.N., Carey, J.M., Ng, K.-Y., Massey, C.I., and Froude, M.J.: Understanding patterns of movement for slow moving landslides. In, Alexander, G.J., and Chin, C.Y. (eds) 20th Symposium of the New Zealand Geotechnical Society, Napier., 2017.

Picarelli, L.: Considerations about the mechanics of slow active landslides in clay. pp. 27-57 (Chapter 3). In, Sassa K, Fukuoka H, Wang F, and Wang G (Eds.), Progress in Landslide Science., 2017.

Rosser, B.J., Dellow, G.D., Haubrock, S.N., and Glassey, P.J.: New Zealand's National Landslide Database, Landslides., 14(6), 1949-1959, 2017.

Skempton, A.W.: Residual Strength of Clays in Landslide, Folded Strata and the Laboratory, Geotechnique., 35, 3-18, 1985.

Stirling, M., McVerry, G., Gerstenberger, M., Litchfield, N., Van Dissen, R., Berryman, K., Barnes, P., Wallace, L., Bradley, B., Villamor, P., Langridge, R., Lamarche, G., Nodder, S., Reyners, M., Rhoades, D., Smith, W., Nicol, A., Pettinga, J., Clark, K., and Jacobs, K.: National Seismic Hazard Model for New Zealand: 2010 Update. Bulletin of the Seismological Society of America, 102, 1514-1542, 2012.

Stout, M.L.: The Utiku landslide, North Island, New Zealand. Geological Society of America: Reviews in Engineering Geology., 3, 171–184, 1977.

Thompson, R.C.: Relationship of geology to slope failures in soft rocks of the Taihape-Mangweka area, Central North Island, New Zealand. PhD Thesis, University of Auckland, 1982.

Valagussa, A., Frattini, P., Crosta, G.B., and Valbuzzi, E.: Pre and post Nepal earthquake landslide inventories. In, Aversa, S.; Cascini, L., Picarelli, L., and Scavia, C. (eds) Landslides and engineered slopes: experience, theory and practice: proceedings of the 12th International Symposium on Landslides. Boca Raton, Fla., 1957-1964, 2016.

van Ash, V Malet, J.P., and Bogaard, T.A.: Problems in predicting the mobility of slow-moving landslides. Engineering Geology., 91, 45-55, 2007.

Wilson, R. C., and Keefer, D.K.: Dynamic analysis of a slope failure from the 6 August 1979 Coyote Lake, California, earthquake, Bulletin of the Seismological Society of America, 73(3), 863–877, 1983.

Earth Surf. Dynam. Discuss., https://doi.org/10.5194/esurf-2018-73
Manuscript under review for journal Earth Surf. Dynam.
Discussion started: 5 October 2018

Table 1: Summary of monotonic drained shear test experiment parameters

Sample Ref	Test stage	Test type	Normal effective stress (kPa)	Strain rate (mm/min^{-1})
UTA	1	Initial shear	400	0.01
UTA	2	Shear reversal	400	0.01
UTB	1	Initial shear	400	0.01
UTB	1	Shear reversal	400	0.01
UTC	1	Initial shear	150	0.01
UTC	2	Shear reversal	150	0.01
UTC	5	Shear reversal	150	0.01

Table 2: Summary of pore pressure reinflation experiment parameters

Sample Ref	Pore pressure experiment	Test stage(s)	Shear surface condition	Confining pressure (kPa)	Initial shear stress	Rate of back pressure change (kPa /hr)	
						Increase	Decrease
UTB	PP1	3/4	Pre-existing	400	95	5	5
UTC	PP1	3/4	Pre-existing	150	52	5	5
UTC	PP2	7-16	Pre-existing	150	52	stepped	Stepped
UTD	PP1	1	Intact	150	52	5	-
UTD	PP2	4	Pre-existing	150	52	5	-

Earth Surf. Dynam. Discuss., https://doi.org/10.5194/esurf-2018-73
Manuscript under review for journal Earth Surf. Dynam.
Discussion started: 5 October 2018

Table 3: Summary of dynamic shear experiment parameters

Sample Ref	Dynamic experiment (DYN)	Test stage	Initial stress		Maximum shear stress per cycle (kPa)	Cycle Frequency (Hz)	Cycle duration (s^{-1})
			Normal (kPa)	Shear (kPa)			
UTC	DYN1	14	150	52	79	1	60
UTE	DYN1	3	150	20	135	1	60
UTE	DYN2	11	150	20	40	1	60
UTE	DYN3	13	150	20	60	1	60
UTE	DYN4	15	150	20	80	1	60
UTE	DYN5	17	150	20	95	1	60
UTF	DYN1	4	150	20	30	2	60
UTF	DYN2	6	150	20	45	2	60
UTF	DYN3	8	150	20	55	2	60
UTF	DYN4	11	150	20	60	2	60
UTF	DYN5	13	150	20	65	2	60
UTF	DYN6	15	150	20	70	2	60
UTF	DYN7	17	150	20	70	2	60
UTF	DYN8	19	150	20	75	2	60
UTF	DYN9	21	150	20	85	2	60
UTF	DYN10	23	150	20	85	2	60
UTF	DYN11	25	150	20	80	2	60
UTF	DYN12	27	150	20	87	2	60
UTF	DYN13	29	150	20	71	2	60
UTF	DYN14	31	150	20	30	2	60

Earth Surf. Dynam. Discuss., https://doi.org/10.5194/esurf-2018-73
Manuscript under review for journal Earth Surf. Dynam.
Discussion started: 5 October 2018

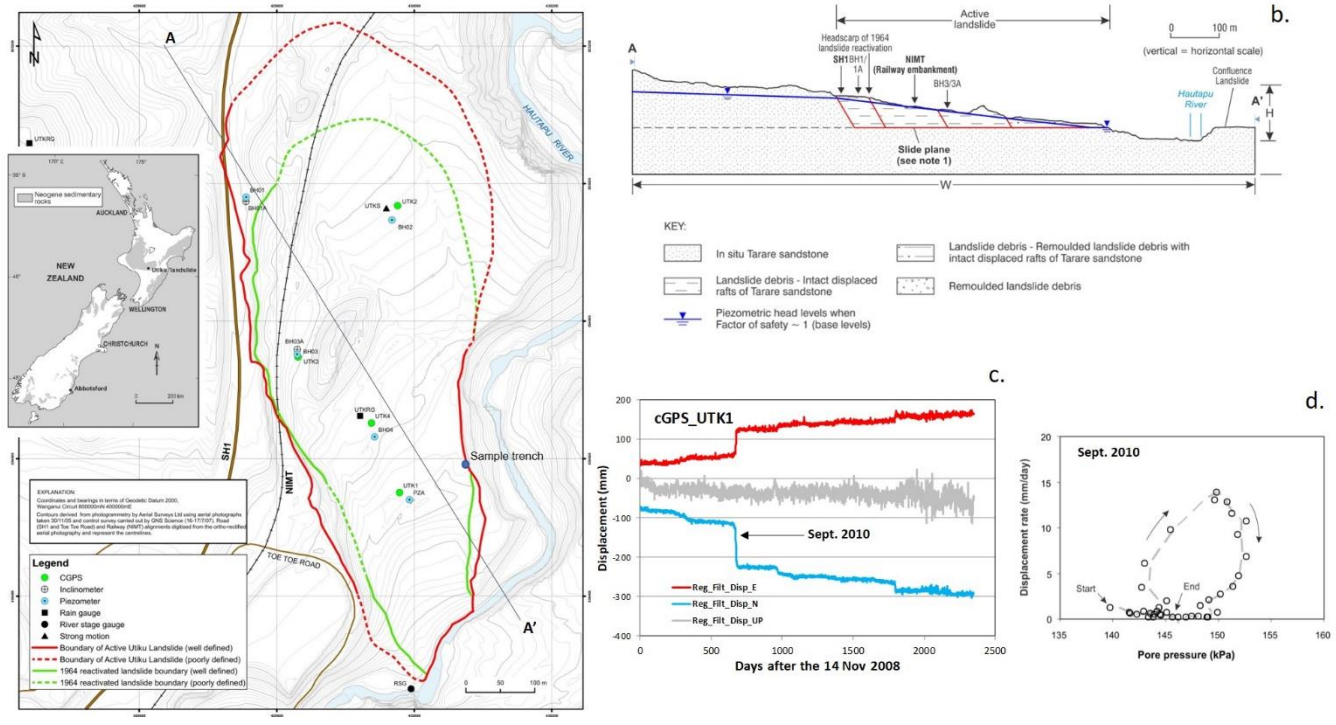

Figure 1: (a) Location of the Utiku landslide in North Island New Zealand, the location of monitoring equipment installed on the landslide in September 2008 and the location of the trench from which samples of the slide surface were taken. (b) Cross section A-A' through the landslide, refer to (a) for the location of the section. (c) Displacement of the continuous GPS (CGPS) UTK1 receiver, showing the displacement towards the east, north and the vertical displacement (UP), from 14 November 2008 to 20 April 2015. Note all displacements are regionally filtered relative to the displacement of CGPS UTKU, which is located off the landslide. (d) the displacement rate estimated along the horizontal vector, derived from the east and north displacement components (CGPS UTK1) for the movement period in September 2010, and the corresponding pore-water pressures recorded at piezometer PZA. All figures are taken and modified from Massey (2010) and Massey et al. (2013).

Earth Surf. Dynam. Discuss., https://doi.org/10.5194/esurf-2018-73
Manuscript under review for journal Earth Surf. Dynam.
Discussion started: 5 October 2018

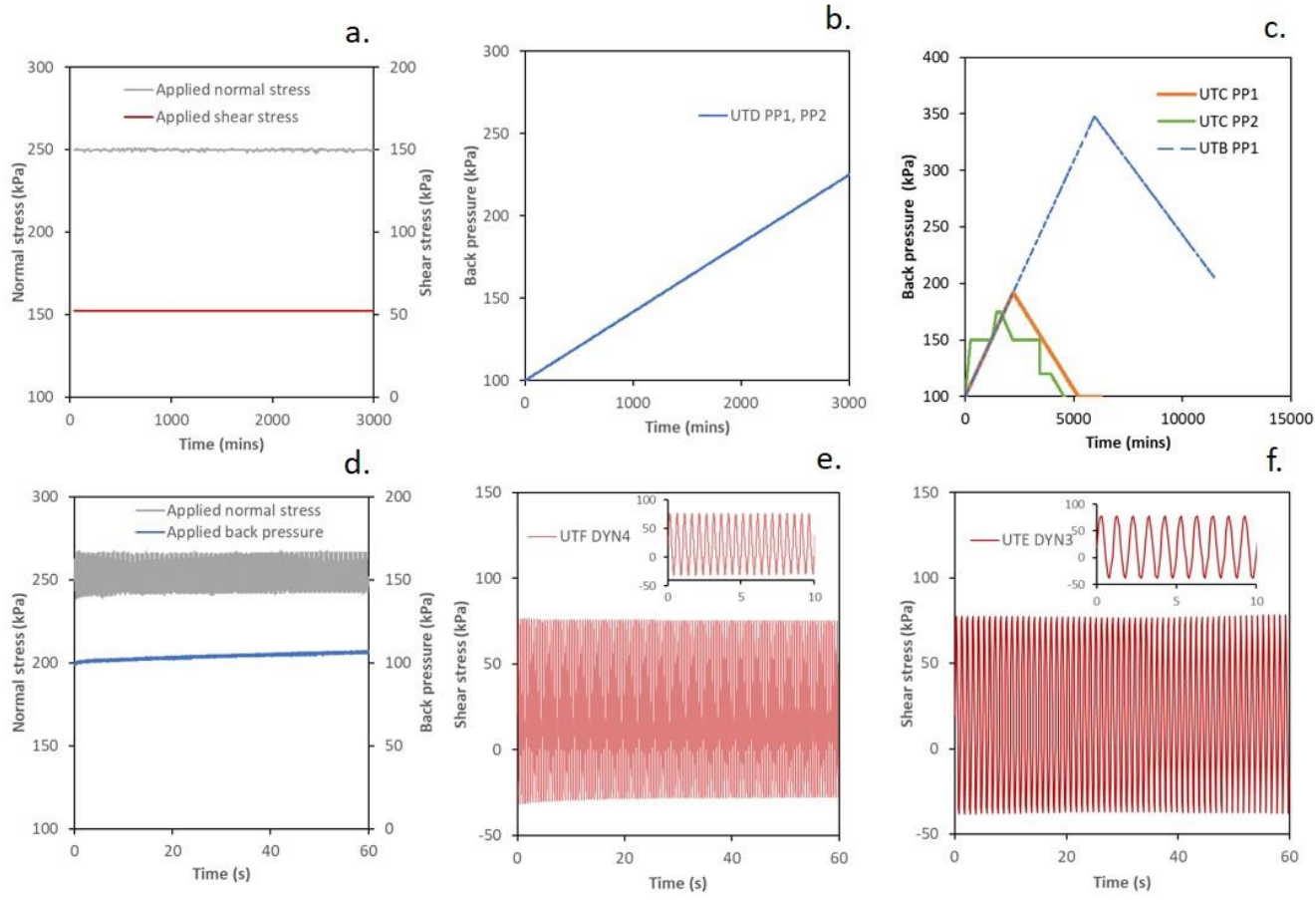

Figure 2: Specialist dynamic shear box experimental approach (a) Constant total normal effective and shear stress applied during pore pressure reinflation experiments conducted from an initial mean effective stress of 150 kPa (b) Linear back pressure increase applied during UTD PP1 and UTD PP2 (c) Linear and stepped increases and decreases in back pressure applied during experiments (d) Constant normal stress and back pressure applied during dynamic shear experiments (e) Dynamic stress controlled shear experiments conducted at a frequency of 2 Hz (f) Dynamic stress controlled shear experiments conducted at a frequency of 1 Hz.

Earth Surf. Dynam. Discuss., https://doi.org/10.5194/esurf-2018-73
Manuscript under review for journal Earth Surf. Dynam.
Discussion started: 5 October 2018

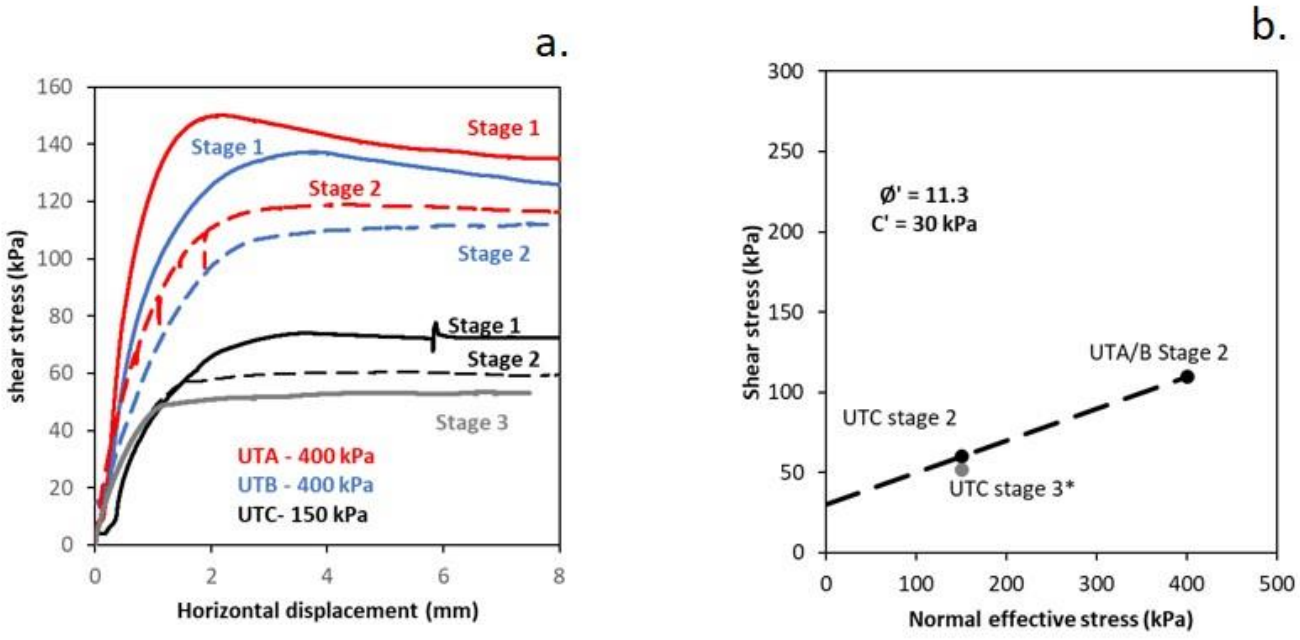

Figure 3: Conventional monotonic drained shear tests (a) stress strain behaviour. (b) monotonic drained failure envelope.

Earth Surf. Dynam. Discuss., https://doi.org/10.5194/esurf-2018-73
Manuscript under review for journal Earth Surf. Dynam.
Discussion started: 5 October 2018

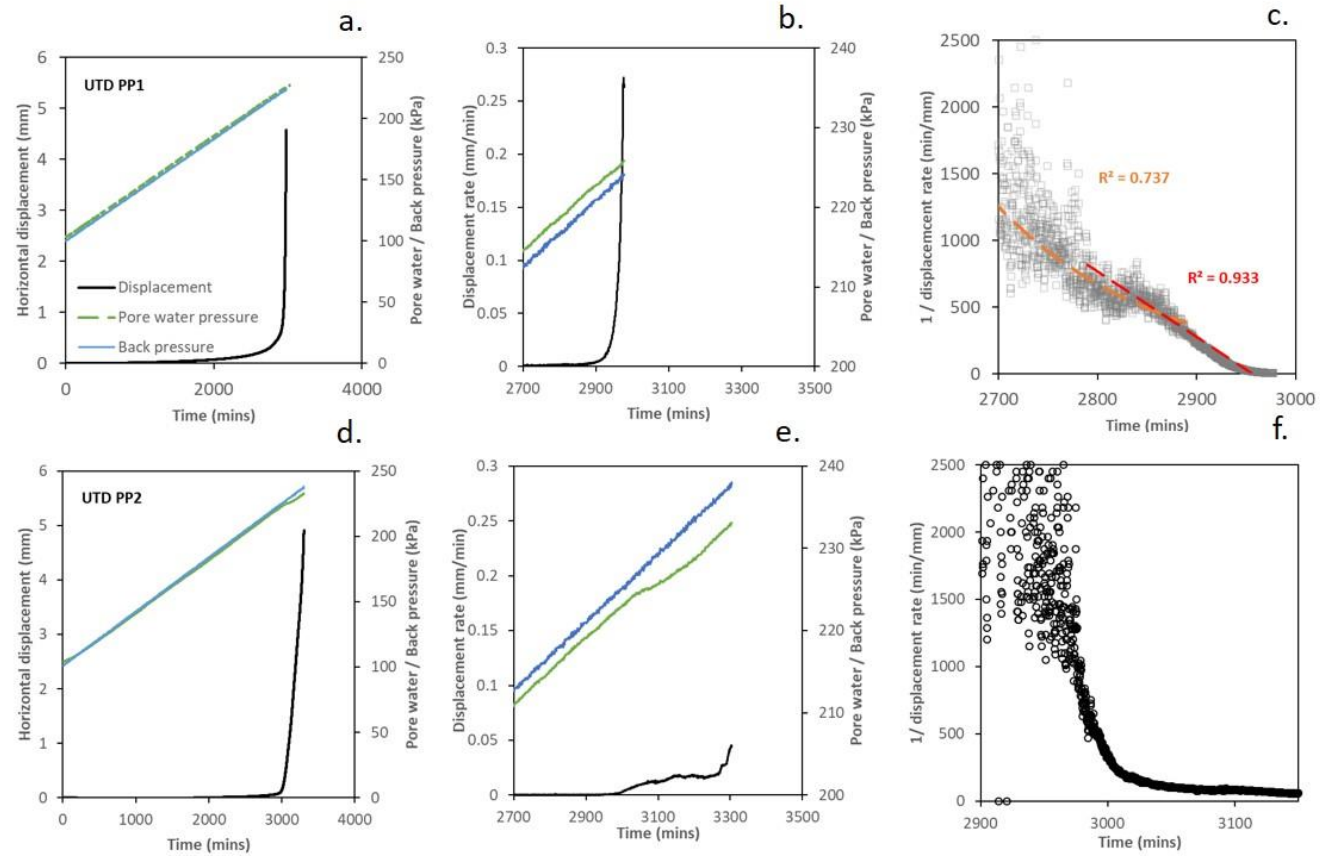

Figure 4: Shear surface displacement behaviour during linearly increase back pressure (applied pore water pressure) on intact (UTD PP1) and remobilised (UTD PP2) shear surface (a) Horizontal displacement against time in relation to the applied back pressure and measured pore water pressure, experiment UTD PP1 (b) Horizontal displacement rate against time in relation to the applied back pressure and measured pore water pressure, experiment UTD PP1 (c) 1/ displacement rate against time, experiment UTD PP1 (d) Horizontal displacement against time in relation to the applied back pressure and measured pore water pressure, experiment UTD PP2 (e) Horizontal displacement rate against time in relation to the applied back pressure and measured pore water pressure, experiment UTD PP2 (f) 1/ displacement rate against time, experiment UTD PP2.

Earth Surf. Dynam. Discuss., https://doi.org/10.5194/esurf-2018-73
Manuscript under review for journal Earth Surf. Dynam.
Discussion started: 5 October 2018

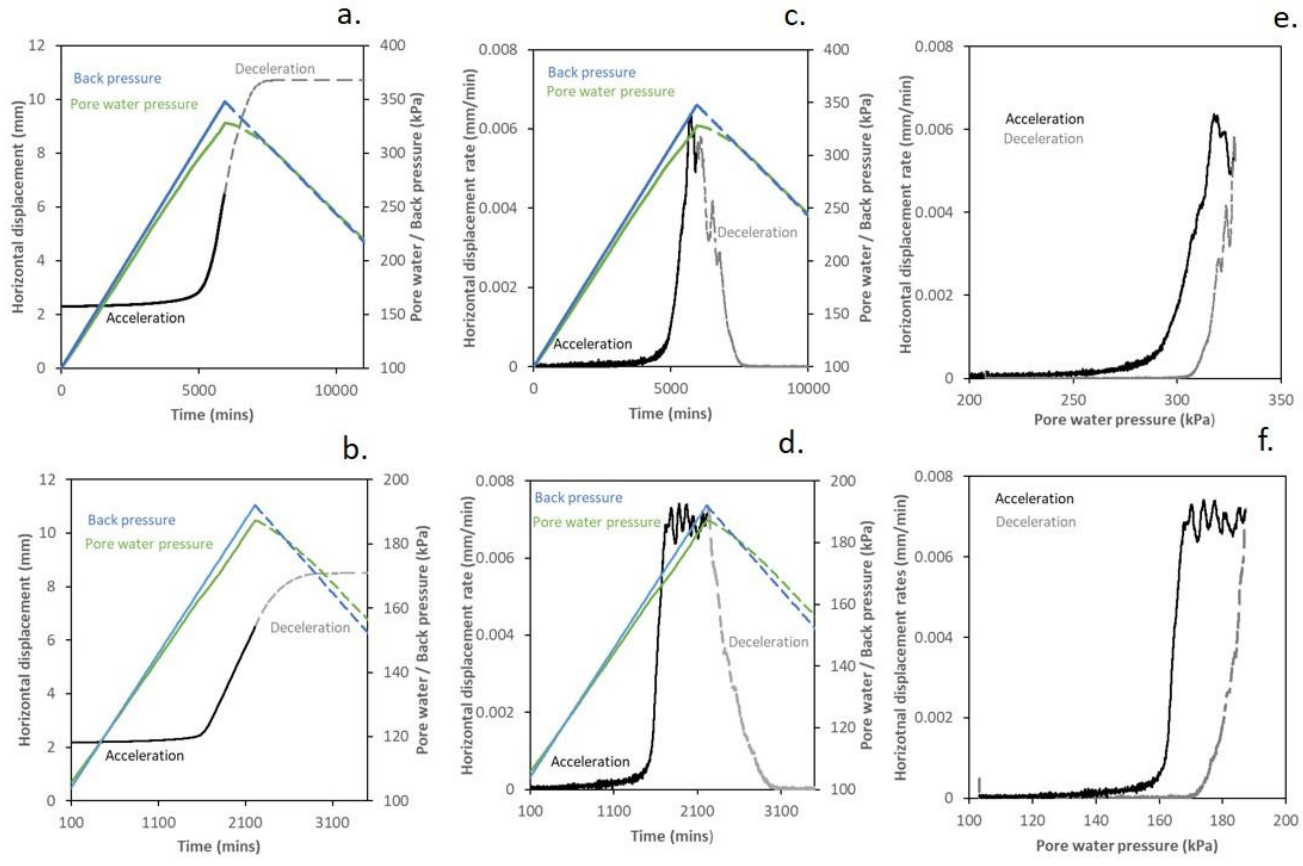

Figure 5: Relationship between shear surface displacement and porewater pressure during linear pore pressure reinflation experiments conducted at mean effective stresses of 400 kPa (UTB PP1) and 150 kPa (UTC PP1) (a) Horizontal displacement against time in relation to the applied back pressure and measured pore water pressure ,experiment UTB PP1 (b) Horizontal displacement against time in relation to the back pressure applied back pressure and measured pore water pressure, experiment UTC PP1 (c) Horizontal displacement rate against time in relation to the applied back pressure and measured pore water pressure, experiment UTB PP1 (d) Horizontal displacement rate against time in relation to the applied back pressure and measured pore water pressure, experiment UTC PP1 (e) Displacement rate against pore water pressure, experiment UTB PP1 (f) Displacement rate against pore water pressure, experiment UTC PP1.

Earth Surf. Dynam. Discuss., https://doi.org/10.5194/esurf-2018-73
Manuscript under review for journal Earth Surf. Dynam.
Discussion started: 5 October 2018

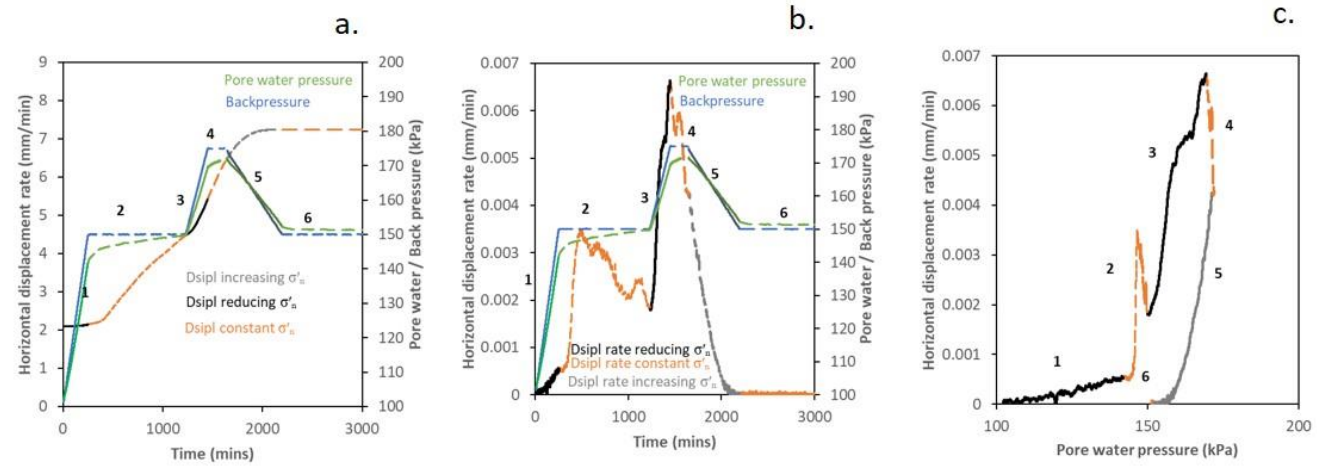

Figure 6: Relationship between shear surface displacement and porewater pressure during stepped pore pressure reinflation experiment conducted at mean effective stresses of 150 kPa (UTC PP2) (a) Horizontal displacement against time in relation to the back pressure applied back pressure and measured pore water pressure, experiment UTC PP2 (b) Horizontal displacement rate against time in relation to the back pressure applied back pressure and measured pore water pressure, experiment UTC PP2 (c) Displacement rate against pore water pressure, experiment UTC PP2.

Earth Surf. Dynam. Discuss., https://doi.org/10.5194/esurf-2018-73
Manuscript under review for journal Earth Surf. Dynam.
Discussion started: 5 October 2018

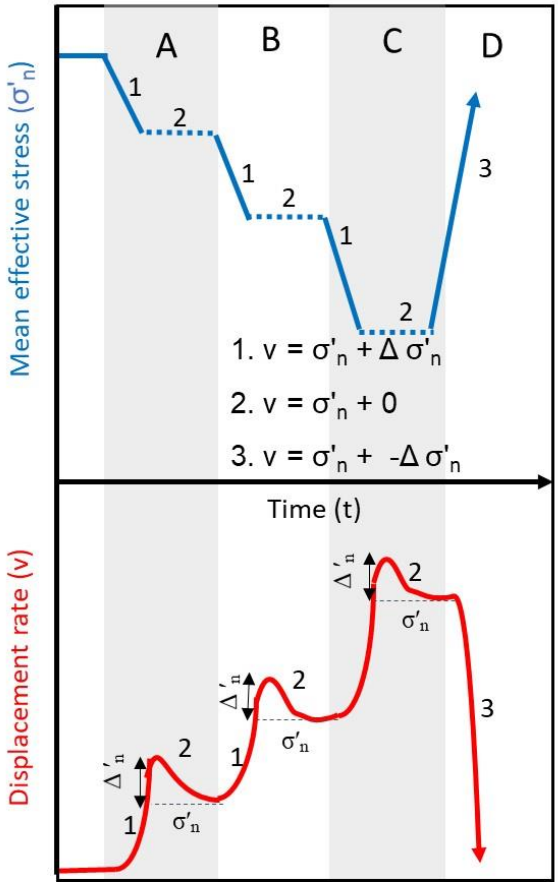

Figure 7: Conceptual model of relationship between displacement rate and mean effective stress in a landslide in response to changes in pore water pressure

Earth Surf. Dynam. Discuss., https://doi.org/10.5194/esurf-2018-73
Manuscript under review for journal Earth Surf. Dynam.
Discussion started: 5 October 2018

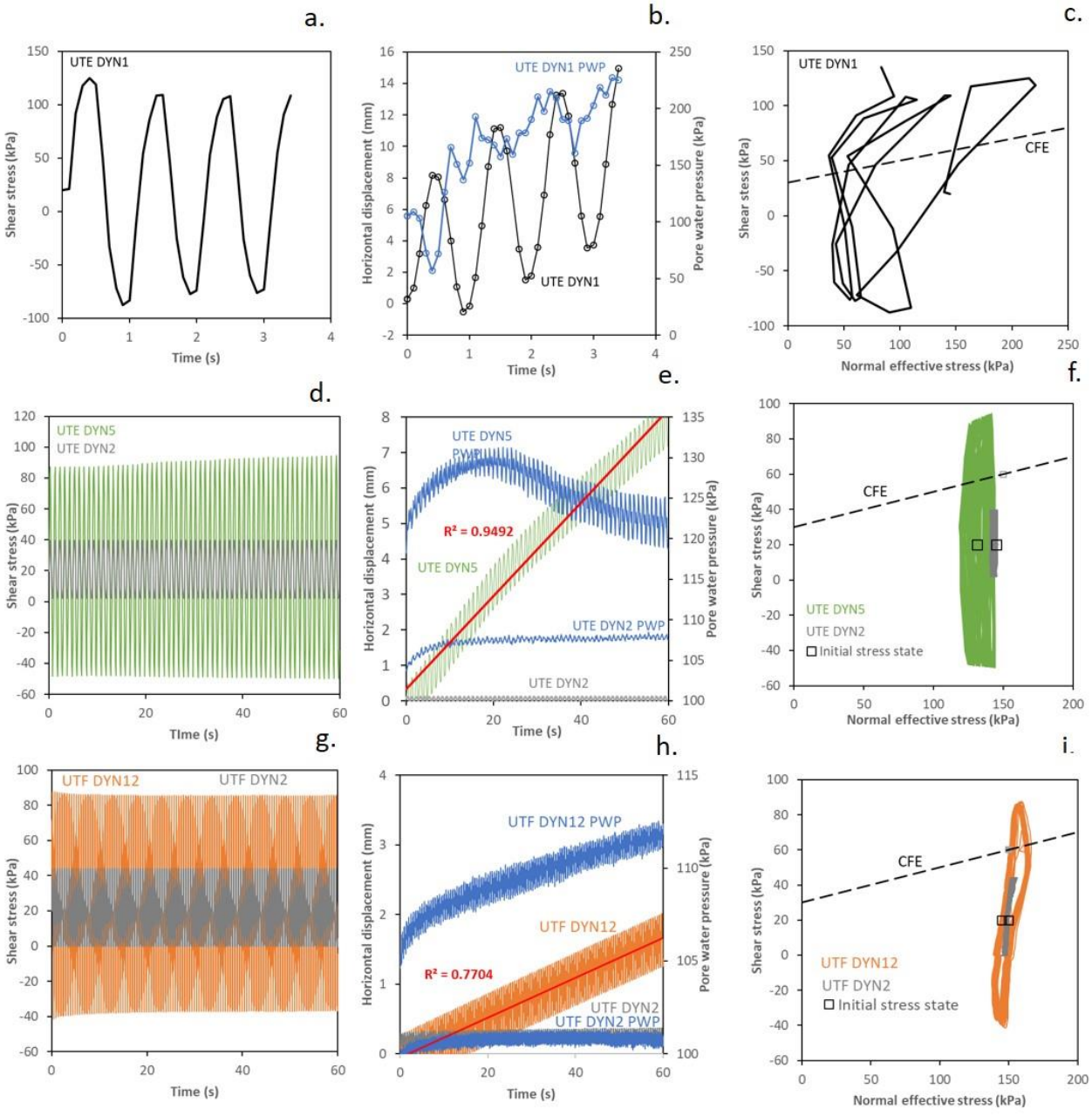

Figure 8: Dynamic shear experiments (a) Dynamic shear stress cycles applied at 1 Hz during experiment UTE DYN1 (b) Displacement and pore-water pressure response measured during experiment UTE DYN1 (c) Sample stress paths in relation to the conventional failure envelope (CFE) during experiment UTE DYN1 (d) Dynamic shear stress cycles applied at 1 Hz experiment UTE DYN2 and UTE DYN5 (e) Displacement and pore-water pressure response measured during experiments UTE DYN2 and UTE DYN5 (f) Sample stress paths in relation to the conventional failure envelope (CFE) during experiments UTE DYN2 and UTE DYN5 (g) Dynamic shear stress cycles applied at 2 Hz during experiment UTF DYN2 and UTF DYN12 (e) Displacement and pore-water pressure response measured during experiments UTE DYN2 and UTE DYN12 (f) Sample stress paths in relation to the conventional failure envelope (CFE) during experiments UTF DYN2 and UTE DYN12.

Earth Surf. Dynam. Discuss., https://doi.org/10.5194/esurf-2018-73
Manuscript under review for journal Earth Surf. Dynam.
Discussion started: 5 October 2018

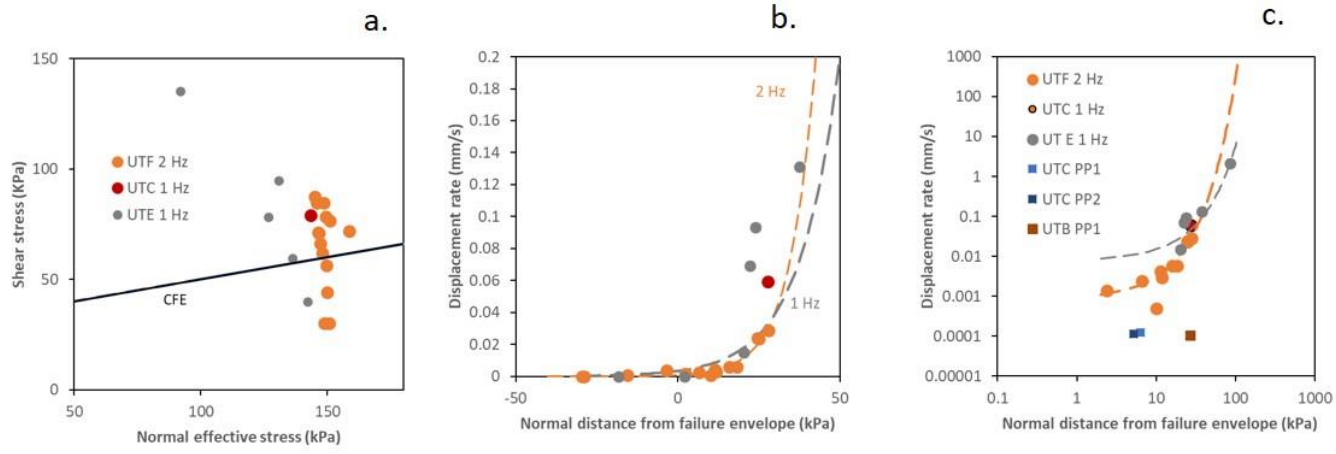

Figure 9: Results of dynamic shear experiments undertaken at 1 Hz and 2Hz (a) Average normal effective stress against maximum shear stress in relation to the conventional failure envelope (CFE) (b) Displacement rate against normal distance from the failure envelope (c) Displacement rate against normal distance from the failure envelope in log scale including pore pressure experiments.

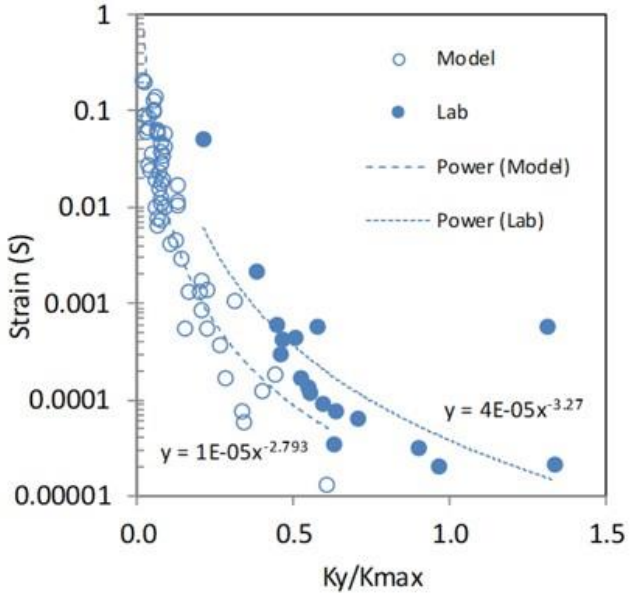

Figure 10: Strain versus Ky/ k_{max} ratios from numerical simulations (hollow circles) and laboratory experiments (solid circles). a) strain at given ratios of the yield acceleration (KY) to the maximum of the average acceleration of the mass (k_{max}), in response to a given dynamic load.